Comprehensive gene expression analysis of organoid-derived healthy human colonic epithelium and cancer cell line by stimulated with live probiotic bacteria

Akira Sen[1,2#], Atsuki Imai[1#], Eiji Miyauchi[1], Kota Yanagisawa[1], Tsukasa Oda[1], Fuki Sasaki[1], Shintaro Uchida[3], Takuhisa Okada[3], Takehiko Yokobori[4], Hiroshi Saeki[3], Toshitaka Odamaki[2], Nobuo Sasaki[1*]

1: The Laboratory for Mucosal Ecosystem Design, Institute for Molecular and Cellular Regulation, Gunma University, Maebashi, Gunma 371-8512, Japan.
2: Innovative Research institute, Morinaga Milk Industry Co Ltd, Zama, Kanagawa 252-8583, Japan
3: Department of General Surgical Science, Gastroenterological Surgery, Gunma University, Graduate School of Medicine, Maebashi, Gunma 371-8511, Japan.
4: Division of Gene Therapy Science, Gunma University, Initiative for Advanced Research (GIAR), Maebashi, Gunma 371-8511, Japan.
#: These authors contributed equally to this work.
*: Correspondence: nosasaki@gunma-u.ac.jp

Abstract

The large intestine has a dense milieu of indigenous bacteria, generating a complex ecosystem with crosstalk between individual bacteria and host cells. *In vitro* host cell modeling and bacterial interactions at the anaerobic interphase have elucidated the crosstalk molecular basis. Although classical cell lines derived from patients with colorectal cancer including Caco-2 are used, whether they adequately mimic normal colonic epithelial physiology is unclear. To address this, we performed transcriptome profiling of Caco-2 and Monolayer-cultured epithelial cells derived from healthy Human Colonic Organoids (MHCO) cultured hemi-anaerobically. Coculture with the anaerobic gut bacteria, *Bifidobacterium longum* subsp. *longum* differentiated the probiotic effects of test cells from those of physiologically normal intestinal and colorectal cancer cells. We cataloged non- or overlapping gene signatures where gene profiles of Caco-2 represented absorptive cells in the small intestinal epithelium, and MHCO showed complete colonic epithelium signature, including stem/progenitor, goblet, and enteroendocrine cells colonocytes. Characteristic gene expression changes related to lipid metabolism, inflammation, and cell-cell adhesion were observed in cocultured live

Bifidobacterium longum and Caco-2 or MHCO. *B. longum*-stimulated MHCO exhibited barrier-enhancing characteristics, as demonstrated in clinical trials. Our data represent a valuable resource for understanding gut microbe and host cell communication.

Keywords

Colon cancer cells, Colonic epithelium, gene expression, gut microbiome, probiotic bacteria, transcriptome profiling

Introduction

The large intestine, also known as the colon, is a crucial component of the human digestive system with a wide range of physiological functions vital for maintaining overall health[1]. One of the primary physiological functions of the colon is the absorption of water and electrolytes from residual undigested food materials entering the colon from the small intestine[2]. The content of the partially digested chyme that passes through the colon is concentrated through water absorption, an essential process that maintains body fluid balance and prevents dehydration.

Additionally, the colon hosts a diverse community of beneficial bacteria, known as the gut microbiota, which contribute significantly to human health[3]. These microorganisms aid in fermenting undigested carbohydrates and breaking down certain substances to produce metabolites, gasses, and vitamins[4]. The gut microbiota plays a crucial role in bolstering the immune system, protecting against harmful pathogens and maintaining the intestinal lining integrity[5]. The role of microorganisms in maintaining homeostasis and influencing various aspects of human physiology has spurred research into probiotics development.

Probiotics are live microorganisms that confer health benefits when consumed in adequate quantities, and they have emerged as a promising strategy for improving human health and well-being[6]. To promote research and development of probiotics, the physiological functions of microorganisms and their effects on the host need to be investigated [7]. However, details of the fundamental molecular mechanisms underlying host cell-bacteria interactions remain largely unknown. Recent improvements in next-generation sequencing and mass spectrometry technologies have increased interest in the trans-omics analysis of gut microbiota. However, the results only provide a correlation between changes in microorganisms and their traits and do not allow direct causal inference. Therefore, *in vitro* models are required to elucidate the detailed

mechanisms of microbe-host cell interactions. However, existing models do not assess the response of normal human intestinal epithelial cells because of the difference in oxygen demands between gut bacteria (most bacteria living in the colon are anaerobes) and host cells (propagate under normoxia).

To overcome this shortcoming, researchers including our group, have developed a state-of-the-art coculture system of human colonic epithelium with highly oxygen-sensitive gut bacteria[8-12]. Colonic epithelial cells were cultured using a two-dimensional (2D) design on the Boyden chamber to establish the coculture system. Immortalized cell lines derived from human colorectal cancer tissue, such as Caco-2 cells, are commonly used to analyze gut bacteria and their metabolites[13]. Although the molecular basis is still unclear, the morphological and biochemical properties of Caco-2 are known to spontaneously transform, converting them into a small intestine-like epithelium following prolonged culture under confluent 2D layer conditions[14]. Consequently, Caco-2 monolayers have been extensively used as *in vitro* models of the small intestine to characterize certain aspects of nutrient uptake [15].

Most probiotic bacteria, such as *Akkermansia* and *Bifidobacterium* species, reside and function in the colon rather than the small intestine[16]. Thus, colonic epithelium must be used in analyzing the role of microbes inhabiting the colon. Recently, normal colonic epithelial cells were stably cultured for extended periods using three-dimensional (3D) mouse and human organoid culture methods[17, 18]. Self-renewing 2D Monolayer-cultured epithelial cells derived from healthy Human Colonic Organoids (MHCO) are also a physiologically relevant model[10, 19]. Moreover, primary cultured intestinal epithelial cells derived from organoids are increasingly used to study intestinal microbes.

In this study, we investigated the feasibility of using organoid-based normal human epithelium instead of Caco-2 in an intestinal hemi-anaerobic coculture system (iHACS)[10] containing the probiotic bacteria, *Bifidobacterium longum*. This system was established to address the limitation of currently available *in vitro* coculture systems of representative human and microbial cells. We conducted a detailed molecular analysis of the differential effects on cell physiology induced by coculture experiments with Caco-2 and normal colonic epithelium. By stimulating a colorectal cancer-derived cell line or normal colonic epithelium with bacteria, we aimed to generate an expression profile for the stratification of probiotic responses.

Results

Characterization of Caco-2 and colonic organoid-derived monolayer

We performed RNA-sequencing (RNA-seq) analysis to decipher the complete genetic information of the intestinal epithelium cultured using iHACS and compared two *in vitro* cell culture models of Caco-2 and 2D cultured normal colonic epithelium derived from MHCO. To collect RNA samples for transcriptome analysis, we first aligned the culture conditions of the Caco-2 and MHCO (Fig. 1A). To collect RNA samples for transcriptome analysis, we first align the culture conditions of Caco-2 and MHCO (Fig. 1A). Caco-2 was found to be able to grow in the organoid-conditioned medium, which is devoid of serum completely, so after 17 days of culture under sufficiently confluent conditions in fetal bovine serum (FBS)-based DMEM Cell Culture Medium[20, 21]. The medium was changed to the organoid-conditioned medium, and RNA was recovered from cells for a further 3 days culture (Fig. 1A). Contrastingly, MHCO were cultured for 3 days after reaching confluence under similar conditions to those used for the Caco-2 (Fig. 1A). Importantly, we comparatively analyzed the gene expression in MHCO and Caco-2 following growth under hemi-anaerobic conditions.

Principal component analysis (PCA) of RNA-seq data from Caco-2 and MHCO cultured using iHACS revealed substantial differences and a clear separation of transcriptional patterns between both samples (Fig. 1B). The transcriptomes of Caco-2 and MHCO differed significantly, and among genes with an expression difference of > 1.5 fold change (adjusted *P*-value [*P*adj] < 0.05), we identified 4,942 and 4,824 genes that were enriched explicitly in Caco-2 and MHCO, respectively (Fig.1C). Furthermore, we visualized two non-overlapping classes of cell type-specific transcripts using hierarchical clustering, Caco-2 specific and MHCO signatures that were expressed in a mutually exclusive manner (Fig. 1D). Among the top 2,000 differentially expressed genes (DEGs), we observed several marker genes of functionally differentiated cells constituting the colonic epithelium: *Keratin 19 (KRT19*, colonocytes), *Mucin 2* (*MUC2*), *Trefoil factor 3* (*TFF3*, goblet cells), and *Chromogranin A*/B (*CHGA and CHGB*, enteroendocrine cells) in the MHCO RNA-seq data (Fig. 1D, E). The stem cell marker gene, *Leucine rich repeat containing G protein-coupled receptor 5* (*LGR5*) was highly expressed in the cancer-derived cell line, whereas other markers of differentiated cells constituting the colonic epithelial tissue were highly expressed in MHCO (Fig. 1E). This finding was further supported by data showing that several known marker genes of the small intestine, such as *Alkaline Phosphatase, intestinal* (*ALPI*)*, Alanyl Aminopeptidase,*

137 *membrane* (*ANPEP*), and *Apolipoprotein B* (*APOB*), were more highly expressed in
138 Caco-2 than they were in MHCO (Fig. 1D, E).
139 Next, the DEGs that differed significantly between Caco-2 and MHCO (Fig 1D)
140 were examined using gene ontology (GO) enrichment analysis. GO analysis of the genes
141 upregulated in cultured Caco-2 showed enrichment of GO terms associated with the Wnt
142 signaling pathway (GO:0016055) and different transport processes, including lipids
143 (GO:0006869), organic anions (GO:0015711) and vitamins (GO:0051180, Fig. 2A). The
144 GO enrichment analysis of Caco-2 showed enrichment of terms related to Wnt signaling
145 pathway and lipids, organic anions, and vitamin transport processes. These findings are
146 consistent with those previously reported on the identity of Caco-2 derived from a patient
147 with colorectal cancer who had a mutation in the *APC* gene. *APC* is a negative regulator
148 of Wnt signaling[22] that induces the expression of the target genes, *LDL Receptor*
149 *Related Protein 1* (*LRP1)*[23], *Dickkopf-1* (*DKK1*)[24], and *Naked cuticle 1* (*NKD1*)[25].
150 Additionally, GO analysis revealed a significant association between the transporters of
151 lipids (apolipoprotein family genes), organic anions (*solute carrier organic anion*
152 *transporter family member* [*SLCO*] family genes), and vitamins (*solute family carrier*
153 [*SLC*] *family*, *NPC1 like intracellular cholesterol transporter 1* [*NPC1L1*], *ATP binding*
154 *cassette subfamily G member 2* [*ABCG2*]) because Caco-2 are an extensively used *in*
155 *vitro* assay for nutrient abruption studies[15] (Fig. 2B).
156 In contrast, genes upregulated in MHCO showed a pronounced enrichment of
157 GO terms related to tissue homeostasis (GO:0001894) involved in goblet cell marker
158 genes (*MUC2* and *TFF3*) and different glycosylation processes, such as protein
159 glycosylation (GO:0006486) and macromolecular glycosylation (GO:0043413) involved
160 in the glycosylation of mucin proteins (*ST6 N-acetylgalactosaminide alpha-2,6-*
161 *sialyltransferase 1* [*ST6GALNAC1*], *beta-1,3-galactosyltransferase 5* [*B3GALT5*], and
162 *Fucosyltransferase 2* [*FUT2*]; Fig. 1E and 2A and C).
163 Furthermore, GO analysis indicated the enrichment of tissue homeostasis genes
164 (GO:0001894) exclusive to MHCO and involved in the mucosal immune system (Fig. 2A).
165 Immune responses to gut bacteria, *Toll-like receptor 4* (*TLR4*)[26], *Aldehyde*
166 *dehydrogenase 1A1* (*ALDH1A1*)[27], and *Polymeric immunoglobulin receptor*
167 (*PIGR*)[28], were detected in MHCO (Fig.2C). Collectively, the presence of these genes
168 and enrichment of relevant GO confirmed that MHCO are more pertinent to observe the
169 physiological response of the colonic epithelium than Caco-2 when those cells were
170 cultured under semi-anaerobic conditions.

171

172 **Response of Caco-2 and MHCO to live anaerobes in the colon**

173 Caco-2 have been used to analyze interactions between host cells and gut bacteria[29],
174 and, therefore, we determined whether the responses of those cells to gut bacteria
175 differed from those of MHCO. To test the physiological effects of commensal anaerobes
176 in the colon, we cocultured Caco-2 or MHCO with a probiotic strain of *B. longum* using
177 iHACS. The incubation time was recently extended to allow the coculture of the intestinal
178 epithelium with anaerobic microbes[10]. Because *Bifidobacterium* is generally localized
179 in the colon, we used healthy MHCOs in this study[30].

180 We confirmed that *B. longum* expression increased similarly in Caco-2 and
181 MHCO cultured with iHACS (Fig. 3A, B). After 24 h, an inoculum of 1×10^7 colony forming
182 units (CFU)/mL of *B. longum* increased to a median of 6.98×10^8 and 8.93×10^8 CFU/mL
183 in coculture with MHCO and Caco-2, respectively ($P = 0.26$, Fig. 3B). RNA was extracted
184 from Caco-2 and MHCO to assess their general responses to the probiotic bacteria. In
185 the PCA of the characterized compound classes in Caco-2 and MHCO in the presence
186 or absence of *B. longum* exposure (Fig. 3C), the first two principal components explained
187 33.8% (PC1) and 17% (PC2) of the total variation. PC1 indicated that MHCO were more
188 distant from the clusters of Caco-2, whereas PC2 showed the response of Caco-2
189 cocultured with *B. longum*. Samples of MHCO alone and cocultured with *B. longum*
190 showed a low variation in each data set (Fig. 3C). Compared to the bacteria-free axenic
191 culture, Caco-2 and MHCO incubated with *B. longum* showed distinct transcriptomic
192 responses, as shown in the volcano plot of replicates exposed to identical conditions (Fig.
193 3D). After filtering for adj$P > 0.05$, the results showed that stimulation with *B. longum*
194 affected the expression of 6,127 genes in Caco-2 by 1.5-fold, consisting of 3,062 and
195 3,065 upregulated and downregulated genes, respectively (Fig. 3D). Similarly, 2,886
196 genes were differentially expressed in MHCO, consisting of 1,407 and 1,479 upregulated
197 and downregulated genes, respectively (Fig. 3D). Additionally, the overlap of
198 upregulated DEGs between MHCO and Caco-2 was minimal, with only 269 commonly
199 expressed genes (Fig 3E). Similarly, 296 DEGs exhibited decreased expression (Fig.
200 3E).

201 The results of the GO analysis of genes that exhibited variations in expression in
202 each cell are shown in Fig. 4. We identified GO terms derived from Caco-2 or MHCO-
203 specific gene expression variations following stimulation with *B. longum*. The DEGs that
204 showed increased expression exclusively in MHCO were predominantly enriched in

205 terms related to lipid metabolism, with the most enriched GO term being lipid transport
206 (GO:0006869) (Fig. 4A). Genes downregulated in MHCO were associated with cell
207 proliferation pathways such as nuclear division (GO:0000280) and chromosome
208 segregation (GO:0007059, Fig. 4B). In Caco-2, the most enriched and least
209 downregulated GO terms were cytoplasmic translation (GO:0002181) and the Wnt
210 signaling pathway (GO:0016055), respectively (Fig. 4C, D). Conversely, most enriched
211 terms in the commonly upregulated genes were associated with lipopolysaccharide (GO:
212 0032496) and response to tumor necrosis factor (GO:0034612 and GO:0071356),
213 whereas downregulated genes were related to double-strand break repair (GO:0006302)
214 (Fig. 4E, F).
215
216 ***B. longum* regulates the expression of transcription factors and genes involved in**
217 **host metabolic pathway**
218 Our analysis of the differentially induced gene expression in Caco-2 and MHCO following
219 bacterial treatment showed a significant increase in the expression of genes involved in
220 peroxisome proliferator-activated receptor (PPAR) signaling in MHCO (Fig. 5A).
221 Furthermore, our transcriptome data showed that the expression of *PPARG* and *PPARA*
222 were upregulated and downregulated in MHCO and Caco-2, respectively following
223 stimulation with *B. longum* (Fig. 5A, B). Genes of signaling pathways associated with
224 PPARs, ketogenesis, lipid transport, cholesterol, fatty acid transporter/oxidation,
225 adipocyte differentiation, and gluconeogenesis were upregulated in MHCO but not in
226 Caco-2 (Fig. 5A).
227 To validate the upregulation of PPAR signaling in MHCO cocultured with *B.*
228 *longum*, we focused on the expression of the PPARA and PPARG target genes. In
229 MHCO coculturing with *B. longum*, *a fatty acid oxidation gene acyl-CoA oxidase 1*
230 (*ACOX1*), a direct target gene of PPARA in the intestine[31], was elevated (Fig. 5B).
231 *Angiopoietin like 4* (*ANGPTL4*), another identical target gene of PPARG in
232 colonocytes[32], was also upregulated in MHCO (Fig. 5B). As expected, gene set
233 enrichment analysis (GSEA) indicated that MHCO, but not Caco-2 cocultured with *B.*
234 *longum* were enriched in genes related to PPAR signaling (normalized enrichment score
235 [*NES*] = 2.06, *adj P* = 0.016 in MHCO, *NES* = -1.15, adj*P* = 0.53, Fig. 5C). These data
236 indicated that live *B. longum* has a potential to activate PAPR signaling on normal
237 physiological conditions of colonic epithelium.
238

239 **Differential inflammatory response to MHCO and Caco-2 to *B. longum* stimulation**
240 Next, we characterized the reaction of each of the cell lines to microbial stimulation by
241 determining their immune responses following stimulation and further investigated gene
242 expression profiles in the production of cytokine and chemokine molecules and their
243 regulators[33]. GSEA revealed that Caco-2 and MHCO stimulated by *B. longum* were
244 commonly enriched for genes associated the NF-κB signaling pathway (NES = 1.91, P
245 < 0.01, adj*P* < 0.05 in MHCO; NES = 2.45, *P* < 0.001, adj*P* < 0.001 in Caco-2; Fig. 6A).
246 To assess the responses of the Caco-2 and MHCO comparatively, we calculated the
247 vehicle control and *B. longum*-induced $\log_2$ fold change (FC) for each gene. As expected,
248 the responses induced by five chemokine genes (*C-C motif chemokine ligand 20*
249 [*CCL20*], *C-X-C motif chemokine ligand 1* [*CXCL1*], *CXCL2*, *CXCL3*, and *CXCL8*)
250 implicated in bacterial sensing[34] showed more pronounced FC values in Caco-2 than
251 in MHCO (Fig. 6B, C).
252 Moreover, bacterial inoculation of Caco-2 and MHCO enhanced the expression
253 of NFKB signaling target genes (*TNFAIP3*, *NFKB inhibitor alpha* [*NFKBIA*], *NFKB*
254 *inhibitor epsilon* [*NFKBIE*], *NFKB inhibitor zeta* [*NFKBIZ*], *RELB proto-oncogene, NF-κB*
255 *subunit* [*RELB*])[35] (Fig. 6B, C). Furthermore, *Interleukin 1A* (*IL-1A*) and *IL-1B*,
256 inflammatory cytokine genes crucial for inflammation and infection defense, were
257 significantly upregulated following coculturing of *B. longum* and MHCO specifically [36]
258 (Fig. 6B, C). Those results suggest that a probiotic microbe, *B. longum,* raises the level
259 of immune surveillance.
260
261 ***B. longum* upregulates intestinal barrier function in MHCO.**
262 We investigated the effect of Bifidobacteria on the intestinal barrier function, by
263 examining the effects on expression patterns of relevant genes. Our RNA-seq results
264 revealed substantial differences in expression patterns of genes related to the mucosal
265 barrier function between Caco-2 and MHCO in response to *B. longum*. The tight junction-
266 related genes, *Claudin 3* (*CLDN3*), *CLDN4,* and *Occludin* (*OCLN*)*,* were upregulated in
267 both Caco-2 and MHCO following exposure to *B. longum*. In contrast, other related
268 genes, *CLDN7* and *Tight junction protein 3* (*TJP3*), were only upregulated in MHCO,
269 whereas *CLDN2* was upregulated in Caco-2 (Fig. 7A, B). Other components of the
270 adherens junction (*Cadherin 1* [*CDH1*], *CDH17*, *Epithelial cell adhesion molecule*
271 [*EPCAM*]) or desmosomes (*Desmoglein 2* [*DSG2*] and *Dystonin* [*DST*]) were linked to a
272 set of genes that were upregulated in *B. longum*-stimulated MHCO and conversely

273 downregulated in Caco-2 (Fig. 7A, C, D). The polarity of intestinal epithelial cells plays a
274 central role in establishing the barrier function for symbiotic relationships with
275 microbiota[37]. The *B. longum*-induced expression pattern of *Integrin subunit α6* (*ITGA6*),
276 a significant factor in the epithelium and basement membrane interaction, also differed
277 between MHCO and Caco-2 (Fig. 7A, E).
278 To investigate whether increased gene expression induced by *B. longum* was
279 associated with improved barrier function, we measured the transepithelial electrical
280 resistance (TEER) in MHCO. Compared to the vehicle control, TEER was significantly
281 increased in cells cocultured with *B. longum* (Fig. 7F). We also evaluated the paracellular
282 permeability of the colonic epithelium using the Lucifer yellow (LY) flux assay with the
283 fluorescent molecule LY, which does not interact with cell components[38]. Consistent
284 with the changes in TEER, LY flux was downregulated when MHCO were cultured with
285 *B. longum* (Fig. 7G). Overall, these results confirmed that probiotic *Bifidobacteria*
286 enhance intestinal barrier integrity through PPARG/STAT3 pathway.
287
288 **Discussion**
289 In this study, we compared gene expression data between Caco-2 and MHCO cultured
290 under hemi-anaerobic conditions to provide valuable datasets for investigating host cells
291 and anaerobic bacteria in the colon. We demonstrated the presence of all cell types that
292 form the colonic epithelium, including stem, goblet, and enteroendocrine cells and
293 colonocytes among the MHCO cultured under hemi-anaerobic conditions. In contrast,
294 the gene expression pattern of Caco-2 was similar to that of epithelial cells of the small
295 intestine, as shown previously[39]. Therefore, MHCO may be a physiologically
296 appropriate model for studying probiotic activities, including of *Bifidobacterium* and
297 *Akkermansia*, in the colon[30, 40].
298 The Caco-2, a cell line generated from a patient with colorectal cancer is the most
299 commonly used in studying the physiological functions of the human intestinal epithelium.
300 These cells spontaneously transform to differentiate and form monolayers of polarized
301 cells with functions similar to those of enterocytes in the small intestine when grown
302 under confluent conditions in Boyden chambers. Consequently, Caco-2 have been
303 widely used to investigate the metabolism and absorption of drugs and nutrients[15, 41].
304 The intestinal environment where enterobacteria are localized is physiologically hypoxic,
305 which affects gene expression patterns through the chromatin state and metabolic
306 pathways[42].

307 Gnotobiotic mice have been the primary animal model used in previous studies
308 of the effect of microbes on hosts. Although studies using in vivo mouse models provide
309 important insights into the physiology of host-microbiome interactions, they are unable
310 to account for significant differences between mice and humans because bacteria exhibit
311 strong species specificity[43]. Conventionally, cell lines derived from patients with cancer
312 have been used to study microbial responses. In this study, healthy primary colonic
313 epithelial cells cultured as organoids and a conventional colorectal cancer-derived cell
314 line were used to examine the physiological response of the host epithelium to microbiota.
315 The gene expression patterns in the DEG analysis in our study indicated that healthy
316 human colonic epithelium derived from organoids was more robust against gut bacteria
317 than the cancer-derived Caco-2 cell line was. These results demonstrated the observed
318 low incidence of overlapping upregulated DEGs between MHCO and Caco-2 and
319 decreased expression of DEGs, indicating that the impact of coculturing with *B. longum*
320 on gene expression was not conserved across these two cell types.
321 Caco-2 have been used to assess the efficacy of probiotics and intestinal bacteria
322 in evaluating mucosal barriers and inflammatory responses. However, two independent
323 reports demonstrated the immunoreactivity of *Faecalibacterium prausnitzii* (recently
324 reclassified as *Faecalibacterium duncaniae*) in host cells using Caco-2 or primary colonic
325 epithelium (organoid)[12, 44]. To the best of our knowledge, this study is the first to
326 evaluate the effect of gut bacteria on Caco-2 and colonic organoids incubated under
327 matched culture and hemi-anaerobic conditions.
328 In this study, the expression of various inflammation-related genes was similarly
329 induced by *B. longum* in Caco-2 and organoid-derived healthy epithelial cells. However,
330 the fold-change ratio was higher in Caco-2 than it was in the organoid cells. This probably
331 occurred because Caco-2 lack goblet cells and poorly express genes such as *MUC2*,
332 which renders the barrier function of the intestinal epithelium vulnerable. Moreover, the
333 bacteria may have more readily caused inflammation in the Caco-2 than in MHCO.
334 Therefore, we focused on immune responses to characterize the reaction of Caco-2 and
335 MHCO to microbial stimulation because genes commonly upregulated in these cell lines
336 show pronounced enrichment of GO terms associated with inflammation. The intestinal
337 epithelium interfaces directly with the external environment and acts as a constant
338 frontline defense for the immune response[45]. Epithelial cells play an essential role in
339 preventing bacterial invasion by producing cytokines and chemokines that determine the
340 nature of the immune response by controlling immune cells. These facts prompted our

341 investigation of gene expression profiles in the production of immune-related molecules
342 and their regulators, including NFKB inhibitors and TNFAIP[33]. The results suggest that
343 the probiotic microbe, *B. longum,* raised levels of immune surveillance.
344 In addition, our GSEA results showing the enrichment of genes related to PPAR
345 signaling in bacterial-stimulated MHCO but not Caco-2 led us to conclude that live *B.*
346 *longum* has the potential to activate PAPR signaling under normal physiological
347 conditions in the colonic epithelium. These observations further confirmed that MHCO
348 are more pertinent for observing the physiological response of the colonic epithelium
349 than Caco-2 are when cultured under semi-anaerobic conditions.
350 Moreover, the results of the TEER analysis corroborated the relationship between
351 *B. longum*-induced increase in gene expression and improved barrier function in MHCO.
352 These observations further confirmed the findings of previous studies in MHCO
353 cocultured with live *B. longum* under hemi-anaerobic culture conditions, which showed
354 that probiotic *Bifidobacteria* enhanced the intestinal barrier integrity through the
355 PPARG/signal transducer and activator of transcription 3 (STAT3) pathway. Previous
356 animal and clinical studies have revealed that *Bifidobacterium*, a probiotic, positively
357 regulates the barrier function of mucosal epithelial cells[46].
358 Epithelial cells are held together by strong anchoring junctions that include tight
359 junctions, adherens junctions, and desmosomes, which are formed by transmembrane
360 adhesion proteins*[47]*. The expression of *CLDN4*, a component of tight junctions, has
361 been shown to be upregulated in the colonic epithelial cells of mice administered
362 *Bifidobacterium[48].* Similarly, our investigation using human colonic organoids
363 cocultured with *B. longum* also showed the upregulation of *CLDN4*. Contrastingly,
364 several molecules related to epithelial cell junctions, such as *CLDN2*, showed conflicting
365 expression patterns in Caco-2 and MHCO stimulated with *B. longum*. *CLDN2* is a pore-
366 forming CLDN that permeates water and ions and has been reported to be elevated in
367 patients with inflammatory bowel disease or neonatal necrotizing enterocolitis[49-52].
368 Furthermore, we found that *CLDN7*, a tight junction-related gene, was upregulated only
369 in MHCO cocultured with *B. longum*. Increased *CLDN2* and decreased *CLDN7* levels
370 have previously been observed in the gastrointestinal tracts of patients with ulcerative
371 colitis[53], and *CLDN7* knockout mice develop colitis spontaneously[54]. In this study, to
372 the best of our knowledge, we provide the first proof that *Bifidobacterium* modulates
373 *CLDN7* expression in the physiologically normal human colonic epithelium.
374 The polarity of intestinal epithelial cells plays a central role in establishing a

barrier function for symbiotic relationships with microbiota[37]. Hemidesmosomes, which are composed of ITGA6T and are a significant factor in the interaction between the epithelium and basement membrane, are expressed at specific junctions in the basal portion of intestinal epithelial cells[55]. In addition to other factors, improvement of the mucus barrier function is a known molecular mechanism in coculture systems. A novel finding of this study is that more genes were altered by bacterial stimulation in Caco-2 than they were in the organoids. While both organoids and Caco-2 share certain variable gene sets, each cell line exhibited a unique variation in the expression of genes linked to inflammation and the mucosal barrier, which are well-known roles of *Bifidobacterium*. However, the potential usefulness and applicability of *Bifidobacterium* needs to be further investigated using appropriate *in vitro* culture systems.

387 **Methods**

388 **Colonic organoid culture**

389 Clinical samples for healthy human colonic organoid establishment and coculturing
390 microbes were obtained from patients at Gunma University Hospital with informed
391 consent after study approval by the ethical committees (HS2022-054). The human
392 colonic organoid was cultured as in the previous report with minor modifications[10].
393 Briefly, three-dimensional colonic organoids were maintained with Modified human
394 colonic organoid (MHCO) medium, consisting of advanced Dulbecco's modified Eagle's
395 medium (DMEM)/F12 supplemented with penicillin/streptomycin, 10mM HEPES, 2 mM
396 Glutamax, 1×B-27 Supplement (Thermo Fisher Scientific), 1 mM N-acetylcysteine
397 (Sigma-Aldrich), 50 ng/mL recombinant mouse epidermal growth factor (Thermo Fisher
398 Scientific), 100 ng/mL mouse recombinant noggin (Peprotech), 1μg/mL human
399 recombinant R-spondin1 (R&D), 500 nM A83-01 (Tocris), 100 ng/mL recombinant
400 human insulin-like growth factor-1 (BioLegend), 50 ng/mL recombinant human fibroblast
401 growth factor-basic (FGF-2) (PeproTech) and conditioned medium containing Wnt3A.
402 The human colonic organoid was derived from a nonpathological biopsy and confirmed
403 by genomic sequencing analysis that it has no driver mutations related to colorectal
404 cancer, as shown in the previous paper[2]. Organoids were passed approximately every
405 5-7 days by physical dissociation using fire-polished Pasteur pipettes. To generate
406 MHCO, ThinCert culture inserts (24-well insert, 0.4 μm pore polyester membrane;
407 Greiner bio-one) were coated with 4% Matrigel diluted with advanced DMEM/F12
408 medium and incubated at 25ºC for 30 minutes, then Matrigel solution was removed. The
409 membrane was dried in a tissue-culture hood for 15 minutes. Human colonic organoids
410 were cultured for 3 to 5 days before being used to plate into monolayer culture in MHCO
411 medium. Three-dimensional cultured organoids were treated with TrypLE Express
412 (Thermo Fisher Scientific) to dissociate into single cells. The cells were resuspended to
413 1× 10^6 cells/mL in MHCO medium containing 10 μM Y-27632 (FUJIFILM Wako Pure
414 Chemical Corporation), and 200 uL of cell suspension was added into the transwell
415 inserts. After 1 day of monolayer culture, MHCO without Y-27632 was used, and the
416 medium was changed every 2 days. When MHCO were cultured in the inserts, MHCO
417 without penicillin/streptomycin was used for their maintenance.

418

419 **Caco-2 culture**

420 The cell line Caco-2 maintained in our group was confirmed by the Cell Line
421 Authentication Service (ATCC). Caco-2 were maintained with the medium consisting of
422 DMEM (high glucose) with L-Glutamine and Phenol Red (FUJIFILM Wako Pure
423 Chemical Corporation) supplemented with 10% heat-treated FBS (Hyclone), MEM Non-
424 Essential Amino Acids Solution (Nacalai tescue), and penicillin/streptomycin. Caco-2
425 cells were passaged approximately 3-5 days before reaching 80% confluency using
426 0.25% Trypsin-EDTA (Gibco) and seeded at 2-4 x10^4 cells/cm^2. 10^5 cells were seeded
427 in transwell culture insert coated Matrigel solution described above. Cells were cultured
428 with the 10% FBS-containing DMEM medium for 17 days. Before the coculture
429 experiment, the culture medium was changed to MHCO medium without antibiotics and
430 cultured for 2 days.
431
432 **Bacterial culture**
433 *B. longum* JCM1217^T (*B. longum*) was obtained from the Riken BioResource Research
434 Center (JCM, Tokyo, Japan). This strain was cultured in modified GAM broth (Nissui
435 Pharmaceutical, Gifu, Japan) for 4 hours at 37ºC under anaerobic conditions using a
436 BACTRON300 anaerobic chamber (Sheldon Manufacturing, Inc., Cornelius, USA). The
437 culture medium was centrifuged (8,000 x g, 1 min, 25ºC) and suspended to
438 approximately 5.0 × 10^7 CFU/mL in a deoxygenated WENRAIF medium supplemented
439 with 100mM HEPES in an anaerobic chamber. Then, 200 uL bacterial suspension was
440 added at the apical side of the transwell in an anaerobic chamber and capped in butyl
441 gum caps. Then, the basolateral side's medium was cultured in a CO2 incubator for 24
442 hours. The number of colony-forming units (CFU) on TOS propionate agar (Yakult
443 Pharmaceutical Industry) was used to calculate the number of live *B. longum*.
444
445 **RNA isolation and sequencing**
446 Total RNA was extracted using the RNeasy Mini Kit (Qiagen) with an RNase-Free DNase
447 Set (Qiagen). Library preparation was performed using Illumina Stranded mRNA Prep
448 and IDT® for Illumina® RNA UD Indexes Set A-B Ligation (Illumina). The concentration
449 and quality of the extracted RNA and adapter-tagged sequence library were calculated
450 using Agilent RNA 6000 Nano and Agilent High Sensitivity DNA Kits (Agilent
451 Technologies), respectively. Sequences were obtained using the NextSeq 1,000 system
452 with the Illumina NextSeq 1000/2000 P2 Reagent kit (100 cycles) (Illumina). Read files
453 were trimmed and mapped to the human reference genome (GRCh38.p.13) using Trim

454 Galore! (ver.0.6.4, https://github.com/FelixKrueger/TrimGalore) and HISAT2 (ver.2.2.1)
455 with default settings[56]. Transcript assembly, GTF document merging, and transcript
456 quantification were performed using Stringtie (ver.2.2.0) [57]. A matrix of read counts
457 mapped to genes was extracted using prepDE.py
458 (http://ccb.jhu.edu/software/stringtie/dl/prepDE.py3).
459

460 **Data analysis and visualization**

461 Normalization from read counts and identifying differentially expressed genes (DEGs)
462 were performed via iterative differential expression analysis (DESeq2) by iDEP1.1
463 software. Adjusted p-value <0.05 and $\log_2$ fold change >1.5 were defined as DEGs.
464 Statistical analysis and data visualization were performed using R (ver.4.3.2). The
465 principal component analysis (PCA) was performed using the 'prcomp' function with TPM
466 matrix in the stats package (ver.3.6.2,
467 https://www.rdocumentation.org/packages/stats/versions/3.6.2) with scaling. The
468 hierarchical clustering and plotting of the heatmap were performed by the 'Heatmap'
469 function in the ComplexHeatmap package (ver.2.18.0,
470 https://github.com/jokergoo/ComplexHeatmap). Functional enrichment analysis of DEGs
471 was performed using the 'enrichGO' function in the clusterProfiler package (ver.4.10.0,
472 https://github.com/YuLab-SMU/clusterProfiler) and GO terms with p-value <0.05 and
473 adjusted p-value <0.05 were considered significant. KEGG pathway enrichment analysis
474 was performed using the 'gseKEGG' function in the clusterProfiler package, and the
475 significantly enriched pathways were defined by nominal adjusted p-value <0.05.
476

477 **Measurement of the integrity of the cell monolayer**

478 The integrity of the cell monolayer was assessed with relative TEER value and LY assay.
479 TEER was measured by Millicell ERS-2 Voltohmmeter (Merck Millipore) following the
480 manufacturer's instruction. Relative TEER was calculated by TEER value after Hemi-
481 Anerobic cultivation for 24 hours relative to their initial value (0 hours). HBSS
482 supplemented with 10mM HEPES, D-PBS(+) Preparation Reagent (Ca, Mg Solution)
483 (Nacalai tesque) were used as transport buffers. After washing the monolayer with
484 transport buffer, 300uL of Lucifer yellow solution (300uM prepared in transport buffer)
485 and 1000uL of transport buffer were added to the apical and basolateral sides of the
486 monolayers, respectively. The monolayers were incubated for 60 minutes in a CO2
487 incubator. After incubation, 200uL of apical and basolateral solution was collected in the

96-well black assay microplate, and the fluorescence was measured at an emission wavelength of 538 nm and excitation at 485 nm using Perkin Elmer Enspire 2300 Multi-mode Microplate Reader with EnSpire Workstation (version 4.13.3005.1482) n=4 biological replicates.

Acknowledgment: The authors thank the members of Gastroenterological Surgery, School of Medical Faculty of Medicine at Gunma University for human sample collection and all members of the laboratory for Mucosal Ecosystem Design for their assistance in experiments and discussion. A Wnt3a-producing cell line was a kind gift from Hans Clevers (Hubrecht Institute).

Funding: This work was supported in part by the Japan Agency for Medical Research and Development (AMED) grant (JP 23ae0121046), JST FOREST program (JPMJFR2161), Grants-in-Aid for the Japanese Society for the Promotion of Science (JSPS) KAKENHI (19H03455, 23H02713), a Grant-in-Aid for Challenging Research (Pioneering, 23K17415), the Astellas Foundation for Research on Metabolic Disorders, and the LOTTE Foundation.

Author contributions:

A.S., A.I., F.S., and T. Odamaki performed all the empirical experiments and analyzed the data. A. S., A. I., K. Y., E. M., and T. Oda. performed and analyzed the RNA-seq data. S.U., T. Okada, T.Y., and H.S. provided tissue specimens. N.S. conceived and conducted the project. A.S. and N.S. wrote the manuscript. All authors discussed the results and edited the manuscript.

Conflict of interest

A. S. and T. O. are employees of Morinaga Milk Industry Co. Ltd. The remaining authors disclose no conflicts.

517 **Figure legends**

518 **Figure 1. Comparison of gene expression profiles between Monolayer cells**
519 **derived from healthy Human Colonic Organoid (MHCO) and Caco-2.**
520 **(A)** A schematic representation of the experiment. **(B)** PCA of the transcriptomes of
521 MHCO and Caco-2. Each plot represents a single transcriptome. Transcriptomes from
522 three replicates were plotted. Ellipses indicate the 95% confidence interval. **(C)**
523 Volcano plot depicting the DEGs of the transcriptomes of MHCO and Caco-2. The x-
524 and the y-axis show the $\log_2$ transformed fold change and the $-\log_{10}$ transformed
525 adjusted p-value. Red and blue dots indicate significantly upregulated genes in MHCO
526 and Caco-2 according to adjusted p-value <0.05 and $\log_2$ fold change >1.5. **(D)**
527 Heatmap depicting the top-2000 DEGs of the transcriptomes of MHCO and Caco-2
528 when sorted by adjusted p-value. **(E)** TPM values of marker genes for each gut
529 epithelial cell type. Data are presented as the mean ± Standard derivatives (SD).
530 Statistical significance was evaluated by Deseq2.
531

532 **Figure 2. GO enrichment analysis of DEGs of the transcriptomes of MHCO and**
533 **Caco-2.**
534 **(A)** Dot plot showing GO terms associated with DEGs for Caco-2 (left panel) and
535 MHCO (right panel) identified in **Figure 1D**. **(B, C)** TPM values of representative genes
536 for each GO term enriched in Caco-2 (**B**) or MHCO (**C**). Data are presented as the
537 mean ± Standard derivatives (SD). Statistical significance was evaluated by Deseq2.
538

539 **Figure 3. Differences in gene expression change among MHCO and Caco-2 after**
540 **coculturing with *B. longum*.**
541 **(A)** A schematic representation of the experiment. **(B)** Colony-forming units (CFU)
542 counts per milliliter of *B. longum* inoculated after 24-hour incubation with MHCO and
543 Caco-2 using iHACS. **(C)** PCA of the transcriptomes of MHCO and Caco-2 cocultured
544 with or without *B. longum*. Each plot represents a single transcriptome. Transcriptomes
545 from three replicates were plotted. Ellipses indicate the 95% confidence interval. **(D)**
546 Volcano plot depicting the upregulated and downregulated genes of Caco-2 (left panel)
547 and MHCO (right panel) after coculturing with *B. longum*. The x- and the y-axis show
548 the $\log_2$ transformed fold change and the $-\log_{10}$ transformed adjusted p-value. Red and
549 blue dots indicate significantly upregulated and downregulated genes after coculturing
550 with *B. longum* according to adjusted p-value <0.05 and $\log_2$ fold change >2. **(E)** Venn

551 diagram comparing the significantly upregulated (left panel) and downregulated genes
552 (right panel) in MHCO or Caco-2 after coculturing with *B. longum*.
553
554 **Figure 4. GO enrichment analysis of upregulated and downregulated genes in**
555 **MHCO and Caco-2 after coculturing with *B. longum*.**
556 **(A-F)** Dot plot showing GO terms associated with upregulated (**A, C, E**) and
557 downregulated genes (**B, D, F**) in MHCO (**A**, **B**), Caco-2 (**C**, **D**), and both (**E**, **F**)
558 identified in Figure 3E.
559
560 **Figure 5. *B. longum* regulates the PPAR signaling pathway.**
561 **(A)** Heatmap of relative expression of PPAR signaling-related genes by co-cultivation
562 of *B. longum* in Caco-2 and MHCO. Statistical significance was evaluated by a Deseq2
563 (*adjusted p-value <0.05, ** adjusted p-value <0.01, *** adjusted p-value <0.001). **(B)**
564 TPM values of representative PPAR receptor and its target genes. Data are presented
565 as the mean ± Standard derivatives (SD). Statistical significance was evaluated by by a
566 Deseq2. **(C)** Enrichment plot of genes in Ppar Signaling Pathway (KEGG) for MHCO
567 (left panel) and Caco-2 (right panel). Each vertical bar represents a gene, and genes
568 enriched in upregulated and downregulated after coculturing with *B. longum* are at the
569 left and right part of the graph, respectively. The normalized enrichment score (NES),
570 the p-value, and the false discovery rate (Adjusted p-value) were indicated in the insert.
571
572 **Figure 6. *B. longum* regulates inflammatory response differently in MHCO and**
573 **Caco-2.**
574 **(A)** Enrichment plot of genes in Nf-Kappa B Signaling Pathway (KEGG) for MHCO (left
575 panel) and Caco-2 (right panel). **(B)** Heatmap of relative expression of inflammatory
576 response-related genes by co-cultivation of *B. longum* in Caco-2 and MHCO. Statistical
577 significance was evaluated by a Deseq2 (*adjusted p-value <0.05, ** adjusted p-value
578 <0.01, *** adjusted p-value <0.001). **(C)** TPM values of representative chemokine, NF-
579 κB related, and inflammatory cytokine genes. Data are presented as the mean ±
580 Standard derivatives (SD). Statistical significance was evaluated by Deseq2.
581
582 **Figure 7. *B. longum* regulates intestinal barrier function.**
583 **(A)** Heatmap of relative expression of cell junction-related genes by co-cultivation of *B.*
584 *longum* in Caco-2 and MHCO. Statistical significance was evaluated by a DESeq2

585 (*adjusted p-value <0.05, ** adjusted p-value <0.01, *** adjusted p-value <0.001). **(B-E)**
586 TPM values of representative tight junction (B), adherence junction (C), desmosome
587 (D), and hemidesmosome (E) related genes. Data are presented as the mean ±
588 Standard derivatives (SD). Statistical significance was evaluated by by a Deseq2. **(F,**
589 **G)** Relative TEER value adjusted by the initial value (**F**) and permeability of Lucifer
590 Yellow (LY) from apical to basolateral compartment (**G**) in MHCO cocultured with *B.*
591 *longum* versus vehicle control. Data are expressed as means ± SD. Statistical
592 significance was evaluated using Welch's t-test.
593

594 **References**

595 [1] J.R. Turner, Intestinal mucosal barrier function in health and disease, Nat Rev Immunol, 9
596 (2009) 799-809.
597 [2] P.R. Kiela, F.K. Ghishan, Physiology of Intestinal Absorption and Secretion, Best Pract Res
598 Clin Gastroenterol, 30 (2016) 145-159.
599 [3] S.V. Lynch, O. Pedersen, The Human Intestinal Microbiome in Health and Disease, N Engl J
600 Med, 375 (2016) 2369-2379.
601 [4] I. Rowland, G. Gibson, A. Heinken, K. Scott, J. Swann, I. Thiele, K. Tuohy, Gut microbiota
602 functions: metabolism of nutrients and other food components, Eur J Nutr, 57 (2018) 1-24.
603 [5] D. Zheng, T. Liwinski, E. Elinav, Interaction between microbiota and immunity in health and
604 disease, Cell Res, 30 (2020) 492-506.
605 [6] M.E. Sanders, D.J. Merenstein, G. Reid, G.R. Gibson, R.A. Rastall, Probiotics and prebiotics
606 in intestinal health and disease: from biology to the clinic, Nat Rev Gastroenterol Hepatol, 16
607 (2019) 605-616.
608 [7] J. Plaza-Diaz, F.J. Ruiz-Ojeda, M. Gil-Campos, A. Gil, Mechanisms of Action of Probiotics,
609 Adv Nutr, 10 (2019) S49-S66.
610 [8] S. Jalili-Firoozinezhad, F.S. Gazzaniga, E.L. Calamari, D.M. Camacho, C.W. Fadel, A. Bein, B.
611 Swenor, B. Nestor, M.J. Cronce, A. Tovaglieri, O. Levy, K.E. Gregory, D.T. Breault, J.M.S. Cabral,
612 D.L. Kasper, R. Novak, D.E. Ingber, A complex human gut microbiome cultured in an anaerobic
613 intestine-on-a-chip, Nat Biomed Eng, 3 (2019) 520-531.
614 [9] R. Kim, P.J. Attayek, Y. Wang, K.L. Furtado, R. Tamayo, C.E. Sims, N.L. Allbritton, An in
615 vitro intestinal platform with a self-sustaining oxygen gradient to study the human
616 gut/microbiome interface, Biofabrication, 12 (2019) 015006.
617 [10] N. Sasaki, K. Miyamoto, K.M. Maslowski, H. Ohno, T. Kanai, T. Sato, Development of a
618 Scalable Coculture System for Gut Anaerobes and Human Colon Epithelium, Gastroenterology,
619 159 (2020) 388-390 e385.
620 [11] P. Shah, J.V. Fritz, E. Glaab, M.S. Desai, K. Greenhalgh, A. Frachet, M. Niegowska, M. Estes,
621 C. Jager, C. Seguin-Devaux, F. Zenhausern, P. Wilmes, A microfluidics-based in vitro model of
622 the gastrointestinal human-microbe interface, Nat Commun, 7 (2016) 11535.
623 [12] J. Zhang, Y.J. Huang, J.Y. Yoon, J. Kemmitt, C. Wright, K. Schneider, P. Sphabmixay, V.
624 Hernandez-Gordillo, S.J. Holcomb, B. Bhushan, G. Rohatgi, K. Benton, D. Carpenter, J.C. Kester,
625 G. Eng, D.T. Breault, O. Yilmaz, M. Taketani, C.A. Voigt, R.L. Carrier, D.L. Trumper, L.G.
626 Griffith, Primary human colonic mucosal barrier crosstalk with super oxygen-sensitive
627 Faecalibacterium prausnitzii in continuous culture, Med, 2 (2021) 74-98 e79.
628 [13] Y. Qi, L. Yu, F. Tian, J. Zhao, Q. Zhai, In vitro models to study human gut-microbiota
629 interactions: Applications, advances, and limitations, Microbiol Res, 270 (2023) 127336.
630 [14] Y. Sambuy, I. De Angelis, G. Ranaldi, M.L. Scarino, A. Stammati, F. Zucco, The Caco-2 cell
631 line as a model of the intestinal barrier: influence of cell and culture-related factors on Caco-2 cell
632 functional characteristics, Cell Biol Toxicol, 21 (2005) 1-26.

633 [15] X. Ding, X. Hu, Y. Chen, J. Xie, M. Ying, Y. Wang, Q. Yu, Differentiated Caco-2 cell models
634 in food-intestine interaction study: Current applications and future trends, Trends in Food
635 Science & Technology, 107 (2021) 455-465.
636 [16] G.P. Donaldson, S.M. Lee, S.K. Mazmanian, Gut biogeography of the bacterial microbiota,
637 Nat Rev Microbiol, 14 (2016) 20-32.
638 [17] T. Sato, D.E. Stange, M. Ferrante, R.G. Vries, J.H. Van Es, S. Van den Brink, W.J. Van Houdt,
639 A. Pronk, J. Van Gorp, P.D. Siersema, H. Clevers, Long-term expansion of epithelial organoids
640 from human colon, adenoma, adenocarcinoma, and Barrett's epithelium, Gastroenterology, 141
641 (2011) 1762-1772.
642 [18] T. Sato, R.G. Vries, H.J. Snippert, M. van de Wetering, N. Barker, D.E. Stange, J.H. van Es,
643 A. Abo, P. Kujala, P.J. Peters, H. Clevers, Single Lgr5 stem cells build crypt-villus structures in
644 vitro without a mesenchymal niche, Nature, 459 (2009) 262-265.
645 [19] Y. Wang, M. DiSalvo, D.B. Gunasekara, J. Dutton, A. Proctor, M.S. Lebhar, I.A. Williamson,
646 J. Speer, R.L. Howard, N.M. Smiddy, S.J. Bultman, C.E. Sims, S.T. Magness, N.L. Allbritton, Self-
647 renewing Monolayer of Primary Colonic or Rectal Epithelial Cells, Cell Mol Gastroenterol Hepatol,
648 4 (2017) 165-182 e167.
649 [20] M. Fujii, M. Matano, K. Toshimitsu, A. Takano, Y. Mikami, S. Nishikori, S. Sugimoto, T.
650 Sato, Human Intestinal Organoids Maintain Self-Renewal Capacity and Cellular Diversity in
651 Niche-Inspired Culture Condition, Cell Stem Cell, 23 (2018) 787-793 e786.
652 [21] C. Jumarie, C. Malo, Caco-2 cells cultured in serum-free medium as a model for the study of
653 enterocytic differentiation in vitro, J Cell Physiol, 149 (1991) 24-33.
654 [22] D. Mouradov, C. Sloggett, R.N. Jorissen, C.G. Love, S. Li, A.W. Burgess, D. Arango, R.L.
655 Strausberg, D. Buchanan, S. Wormald, L. O'Connor, J.L. Wilding, D. Bicknell, I.P. Tomlinson,
656 W.F. Bodmer, J.M. Mariadason, O.M. Sieber, Colorectal cancer cell lines are representative
657 models of the main molecular subtypes of primary cancer, Cancer Res, 74 (2014) 3238-3247.
658 [23] B.E. Michels, M.H. Mosa, B.M. Grebbin, D. Yepes, T. Darvishi, J. Hausmann, H. Urlaub, S.
659 Zeuzem, H.M. Kvasnicka, T. Oellerich, H.F. Farin, Human colon organoids reveal distinct
660 physiologic and oncogenic Wnt responses, J Exp Med, 216 (2019) 704-720.
661 [24] A. Niida, T. Hiroko, M. Kasai, Y. Furukawa, Y. Nakamura, Y. Suzuki, S. Sugano, T. Akiyama,
662 DKK1, a negative regulator of Wnt signaling, is a target of the beta-catenin/TCF pathway,
663 Oncogene, 23 (2004) 8520-8526.
664 [25] D. Yan, M. Wiesmann, M. Rohan, V. Chan, A.B. Jefferson, L. Guo, D. Sakamoto, R.H.
665 Caothien, J.H. Fuller, C. Reinhard, P.D. Garcia, F.M. Randazzo, J. Escobedo, W.J. Fantl, L.T.
666 Williams, Elevated expression of axin2 and hnkd mRNA provides evidence that Wnt/beta -catenin
667 signaling is activated in human colon tumors, Proc Natl Acad Sci U S A, 98 (2001) 14973-14978.
668 [26] J.F. Burgueno, M.T. Abreu, Epithelial Toll-like receptors and their role in gut homeostasis
669 and disease, Nat Rev Gastroenterol Hepatol, 17 (2020) 263-278.
670 [27] J.A. Hall, J.R. Grainger, S.P. Spencer, Y. Belkaid, The role of retinoic acid in tolerance and
671 immunity, Immunity, 35 (2011) 13-22.

672 [28] F.E. Johansen, C.S. Kaetzel, Regulation of the polymeric immunoglobulin receptor and IgA
673 transport: new advances in environmental factors that stimulate pIgR expression and its role in
674 mucosal immunity, Mucosal Immunol, 4 (2011) 598-602.
675 [29] R. McCoy, S. Oldroyd, W. Yang, K. Wang, D. Hoven, D. Bulmer, M. Zilbauer, R.M. Owens,
676 In Vitro Models for Investigating Intestinal Host-Pathogen Interactions, Adv Sci (Weinh), 11
677 (2024) e2306727.
678 [30] M. Derrien, F. Turroni, M. Ventura, D. van Sinderen, Insights into endogenous
679 Bifidobacterium species in the human gut microbiota during adulthood, Trends Microbiol, 30
680 (2022) 940-947.
681 [31] Y. Luo, C. Xie, C.N. Brocker, J. Fan, X. Wu, L. Feng, Q. Wang, J. Zhao, D. Lu, M. Tandon,
682 M. Cam, K.W. Krausz, W. Liu, F.J. Gonzalez, Intestinal PPARalpha Protects Against Colon
683 Carcinogenesis via Regulation of Methyltransferases DNMT1 and PRMT6, Gastroenterology, 157
684 (2019) 744-759 e744.
685 [32] S. Kersten, S. Mandard, N.S. Tan, P. Escher, D. Metzger, P. Chambon, F.J. Gonzalez, B.
686 Desvergne, W. Wahli, Characterization of the fasting-induced adipose factor FIAF, a novel
687 peroxisome proliferator-activated receptor target gene, J Biol Chem, 275 (2000) 28488-28493.
688 [33] M.M. Rahman, G. McFadden, Modulation of NF-kappaB signalling by microbial pathogens,
689 Nat Rev Microbiol, 9 (2011) 291-306.
690 [34] M. Friedrich, M. Pohin, F. Powrie, Cytokine Networks in the Pathophysiology of
691 Inflammatory Bowel Disease, Immunity, 50 (2019) 992-1006.
692 [35] G.D. Bren, N.J. Solan, H. Miyoshi, K.N. Pennington, L.J. Pobst, C.V. Paya, Transcription of
693 the RelB gene is regulated by NF-kappaB, Oncogene, 20 (2001) 7722-7733.
694 [36] A. Mantovani, C.A. Dinarello, M. Molgora, C. Garlanda, Interleukin-1 and Related Cytokines
695 in the Regulation of Inflammation and Immunity, Immunity, 50 (2019) 778-795.
696 [37] M.A. McGuckin, R. Eri, L.A. Simms, T.H. Florin, G. Radford-Smith, Intestinal barrier
697 dysfunction in inflammatory bowel diseases, Inflamm Bowel Dis, 15 (2009) 100-113.
698 [38] E.E. Marr, T.J. Mulhern, M. Welch, P. Keegan, C. Caballero-Franco, B.G. Johnson, M.
699 Kasaian, H. Azizgolshani, T. Petrie, J. Charest, E. Wiellette, A platform to reproducibly evaluate
700 human colon permeability and damage, Sci Rep, 13 (2023) 8922.
701 [39] K. Kulthong, G. Hooiveld, L. Duivenvoorde, I. Miro Estruch, V. Marin, M. van der Zande, H.
702 Bouwmeester, Transcriptome comparisons of in vitro intestinal epithelia grown under static and
703 microfluidic gut-on-chip conditions with in vivo human epithelia, Sci Rep, 11 (2021) 3234.
704 [40] D. Cheng, M.Z. Xie, A review of a potential and promising probiotic candidate-Akkermansia
705 muciniphila, J Appl Microbiol, 130 (2021) 1813-1822.
706 [41] N. Panse, P.M. Gerk, The Caco-2 Model: Modifications and enhancements to improve
707 efficiency and predictive performance, Int J Pharm, 624 (2022) 122004.
708 [42] R.G. Bristow, R.P. Hill, Hypoxia and metabolism. Hypoxia, DNA repair and genetic
709 instability, Nat Rev Cancer, 8 (2008) 180-192.
710 [43] E.K. Mallott, K.R. Amato, Host specificity of the gut microbiome, Nat Rev Microbiol, 19

711 (2021) 639-653.
712 [44] M. Sadaghian Sadabad, J.Z. von Martels, M.T. Khan, T. Blokzijl, G. Paglia, G. Dijkstra, H.J.
713 Harmsen, K.N. Faber, A simple coculture system shows mutualism between anaerobic
714 faecalibacteria and epithelial Caco-2 cells, Sci Rep, 5 (2015) 17906.
715 [45] J.M. Allaire, S.M. Crowley, H.T. Law, S.Y. Chang, H.J. Ko, B.A. Vallance, The Intestinal
716 Epithelium: Central Coordinator of Mucosal Immunity, Trends Immunol, 39 (2018) 677-696.
717 [46] R. Abdulqadir, J. Engers, R. Al-Sadi, Role of Bifidobacterium in Modulating the Intestinal
718 Epithelial Tight Junction Barrier: Current Knowledge and Perspectives, Curr Dev Nutr, 7 (2023)
719 102026.
720 [47] M.A. Garcia, W.J. Nelson, N. Chavez, Cell-Cell Junctions Organize Structural and Signaling
721 Networks, Cold Spring Harb Perspect Biol, 10 (2018).
722 [48] X. Shu, J. Wang, L. Zhao, J. Wang, P. Wang, F. Zhang, R. Wang, Bifidobacterium lactis TY-
723 S01 protects against alcoholic liver injury in mice by regulating intestinal barrier function and gut
724 microbiota, Heliyon, 9 (2023) e17878.
725 [49] K.R. Bergmann, S.X. Liu, R. Tian, A. Kushnir, J.R. Turner, H.L. Li, P.M. Chou, C.R. Weber,
726 I.G. De Plaen, Bifidobacteria stabilize claudins at tight junctions and prevent intestinal barrier
727 dysfunction in mouse necrotizing enterocolitis, Am J Pathol, 182 (2013) 1595-1606.
728 [50] A. Horowitz, S.D. Chanez-Paredes, X. Haest, J.R. Turner, Paracellular permeability and tight
729 junction regulation in gut health and disease, Nat Rev Gastroenterol Hepatol, 20 (2023) 417-432.
730 [51] S. Prasad, R. Mingrino, K. Kaukinen, K.L. Hayes, R.M. Powell, T.T. MacDonald, J.E. Collins,
731 Inflammatory processes have differential effects on claudins 2, 3 and 4 in colonic epithelial cells,
732 Lab Invest, 85 (2005) 1139-1162.
733 [52] S. Zeissig, N. Burgel, D. Gunzel, J. Richter, J. Mankertz, U. Wahnschaffe, A.J. Kroesen, M.
734 Zeitz, M. Fromm, J.D. Schulzke, Changes in expression and distribution of claudin 2, 5 and 8 lead
735 to discontinuous tight junctions and barrier dysfunction in active Crohn's disease, Gut, 56 (2007)
736 61-72.
737 [53] T. Oshima, H. Miwa, T. Joh, Changes in the expression of claudins in active ulcerative colitis,
738 J Gastroenterol Hepatol, 23 Suppl 2 (2008) S146-150.
739 [54] L. Ding, Z. Lu, O. Foreman, R. Tatum, Q. Lu, R. Renegar, J. Cao, Y.H. Chen, Inflammation
740 and disruption of the mucosal architecture in claudin-7-deficient mice, Gastroenterology, 142
741 (2012) 305-315.
742 [55] J. Stutzmann, A. Bellissent-Waydelich, L. Fontao, J.F. Launay, P. Simon-Assmann, Adhesion
743 complexes implicated in intestinal epithelial cell-matrix interactions, Microsc Res Tech, 51 (2000)
744 179-190.
745 [56] D. Kim, J.M. Paggi, C. Park, C. Bennett, S.L. Salzberg, Graph-based genome alignment and
746 genotyping with HISAT2 and HISAT-genotype, Nat Biotechnol, 37 (2019) 907-915.
747 [57] M. Pertea, G.M. Pertea, C.M. Antonescu, T.C. Chang, J.T. Mendell, S.L. Salzberg, StringTie
748 enables improved reconstruction of a transcriptome from RNA-seq reads, Nat Biotechnol, 33
749 (2015) 290-295.

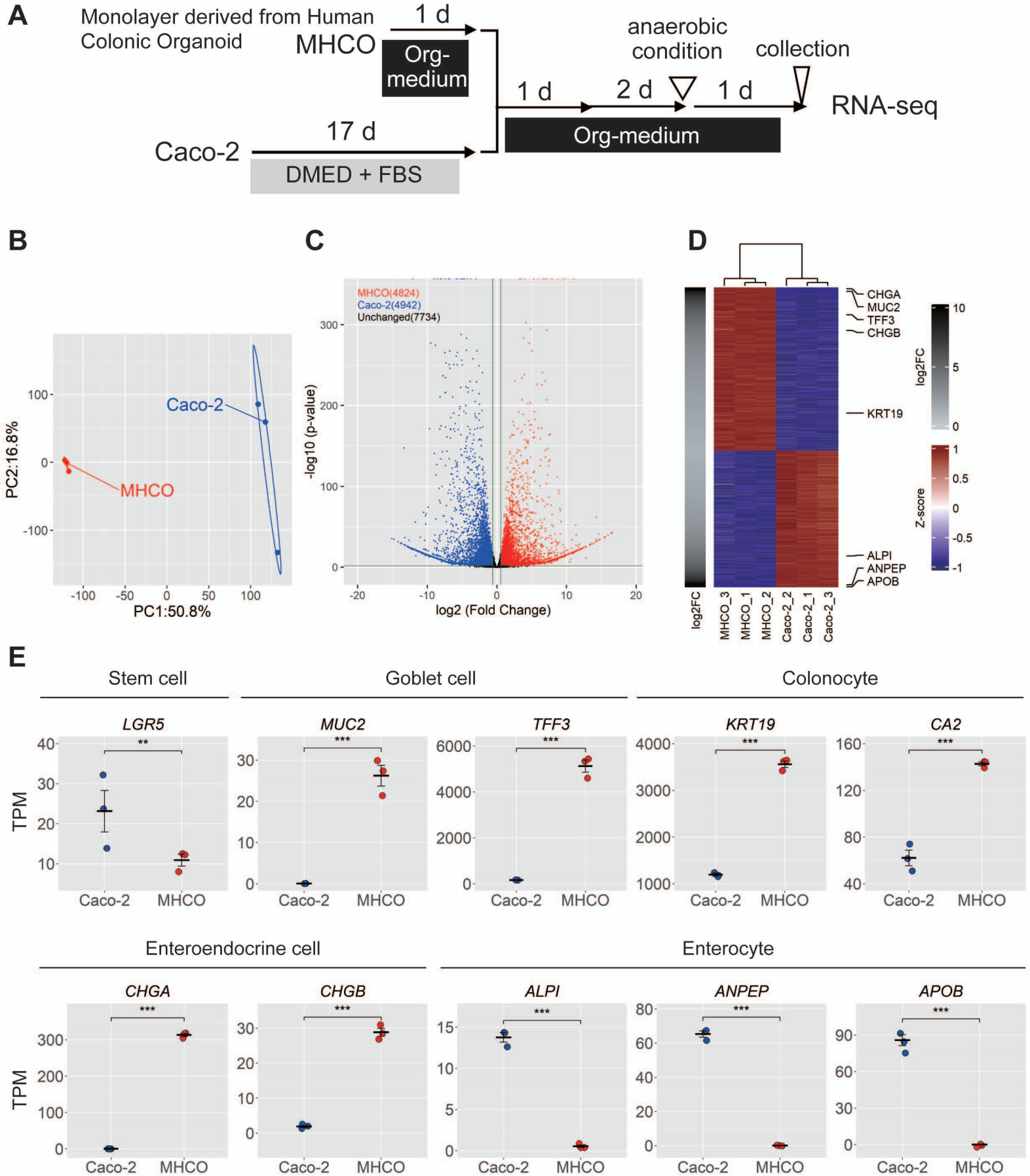

Figure 1. Sen et al.

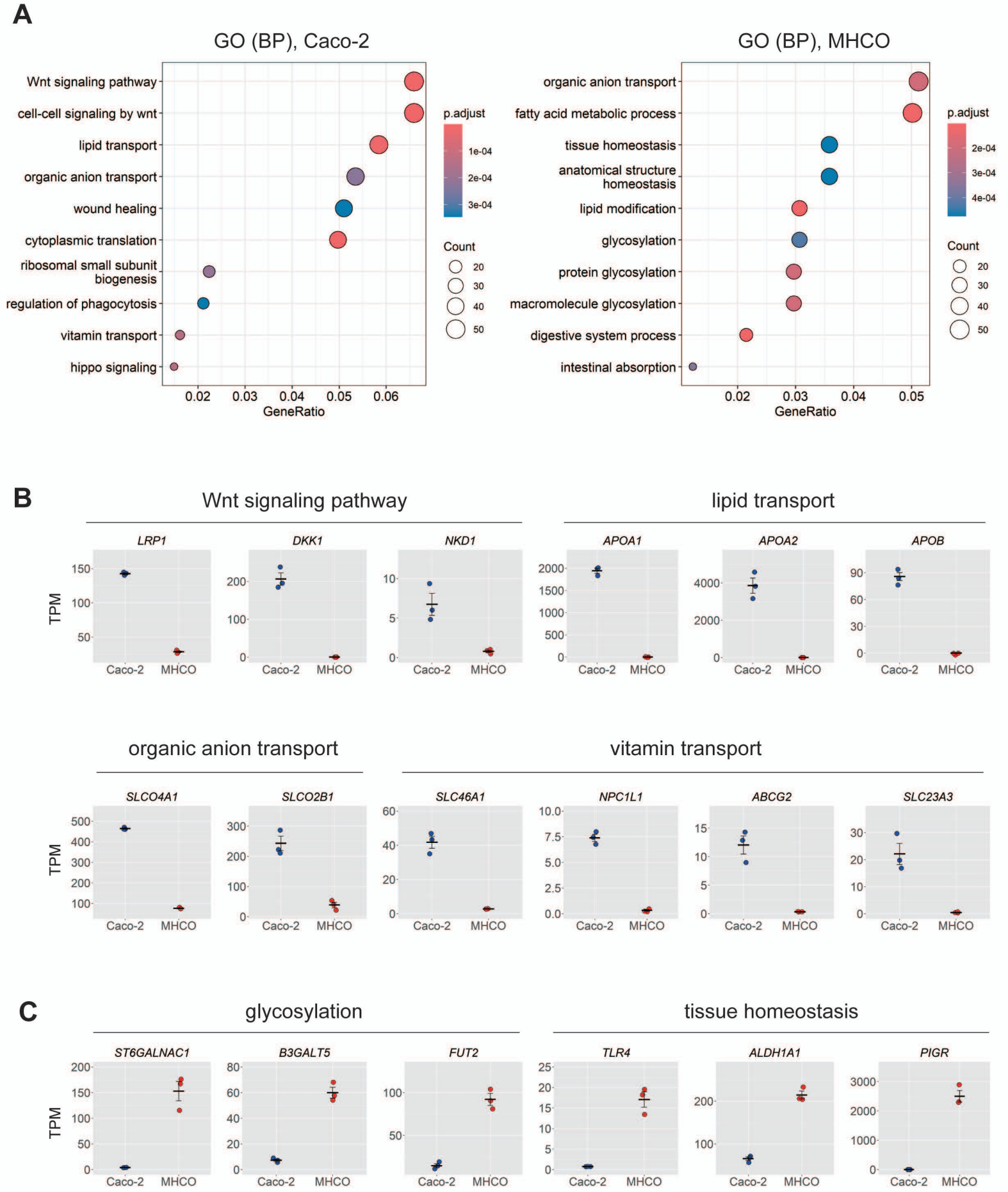

Figure 2. Sen et al.

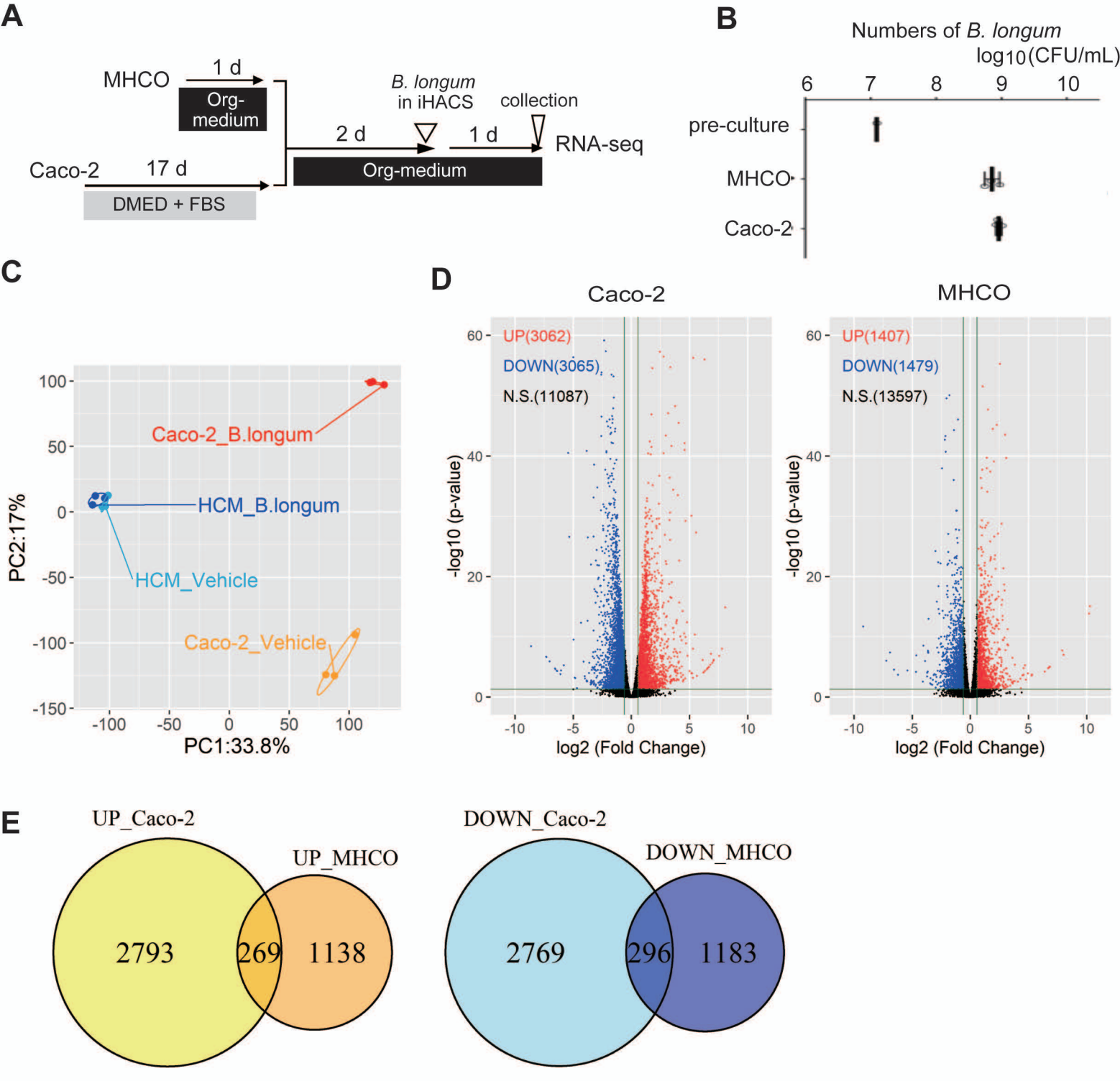

Figure 3. Sen et al.

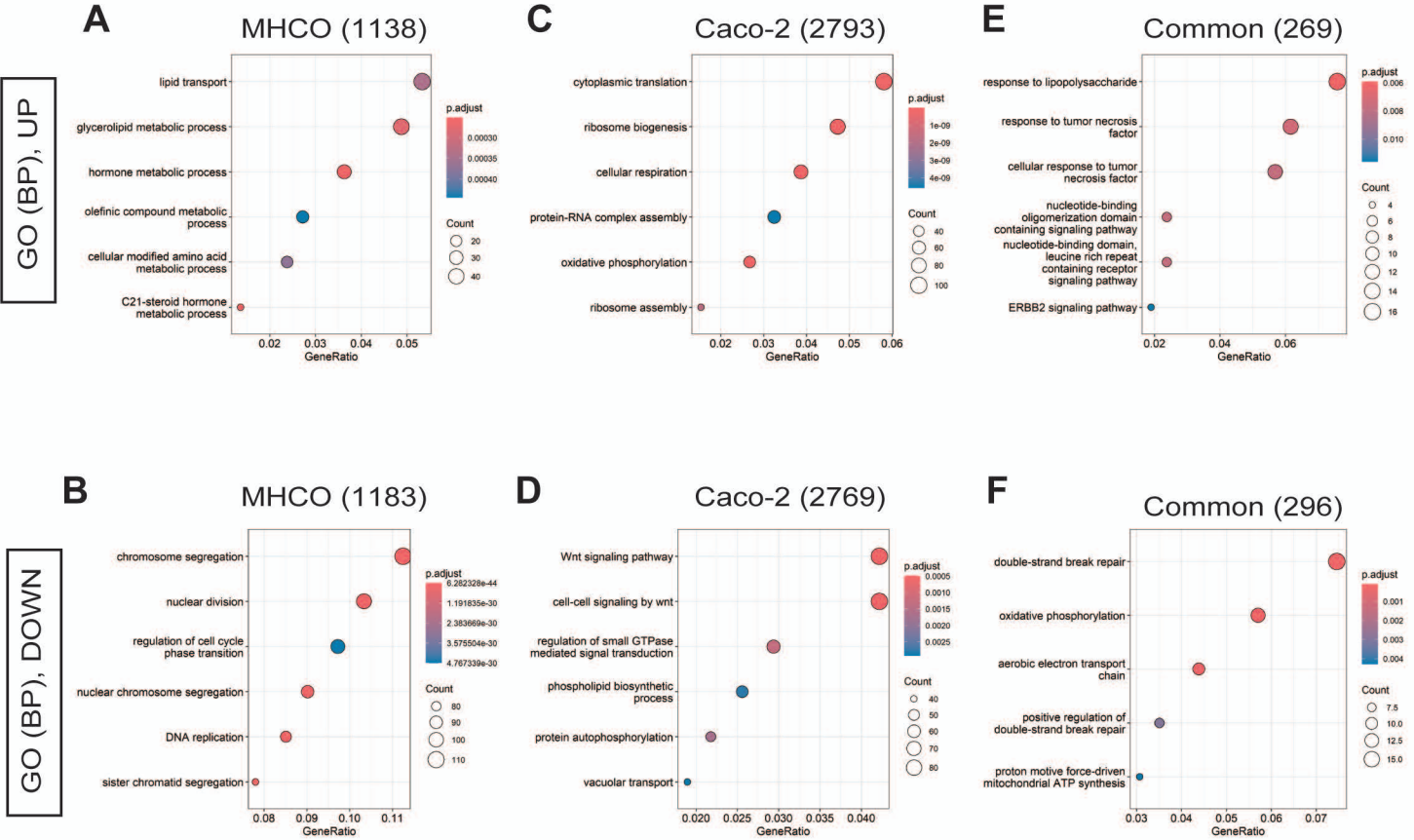

Figure 4. Sen et al.

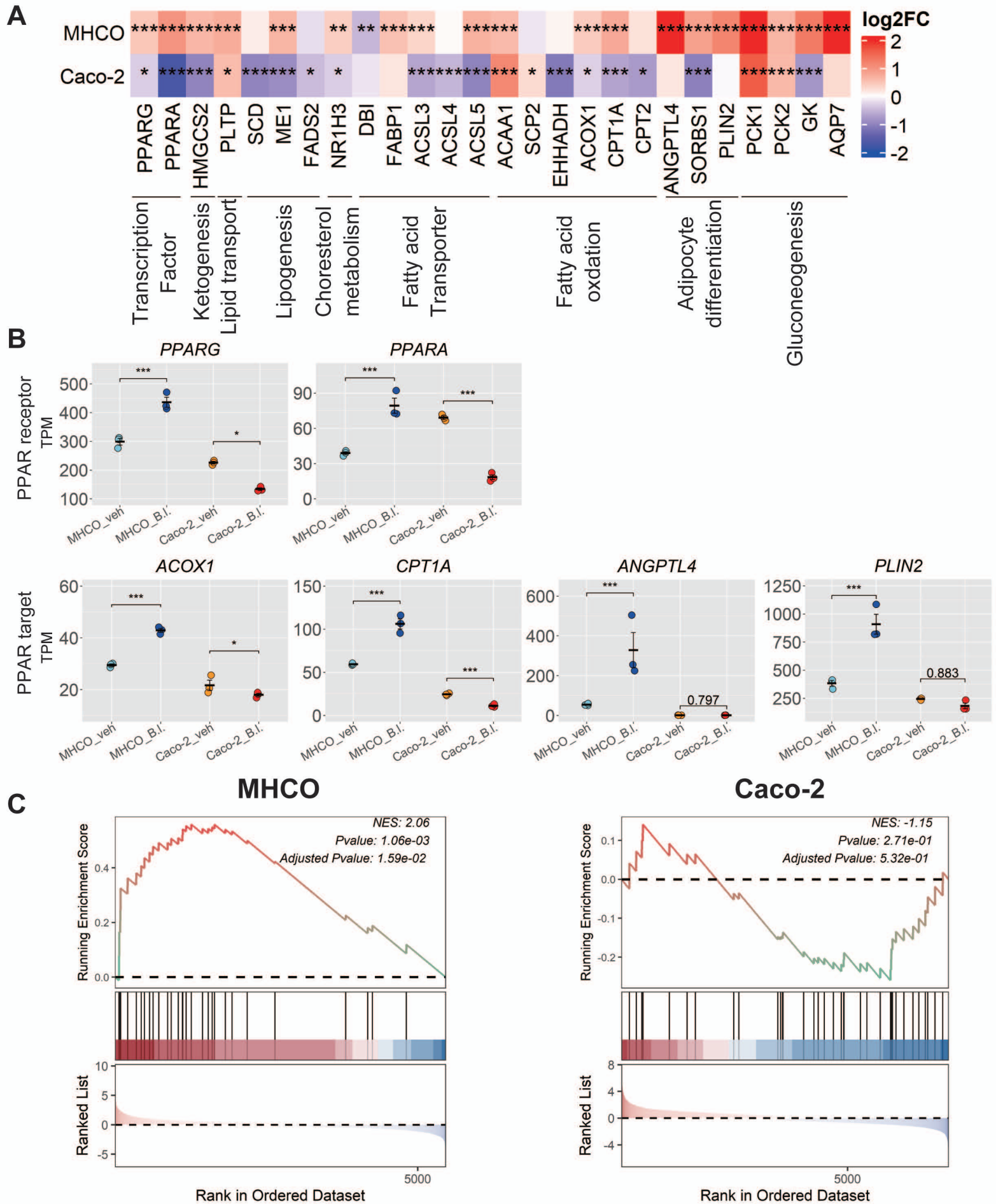

Figure 5. Sen et al.

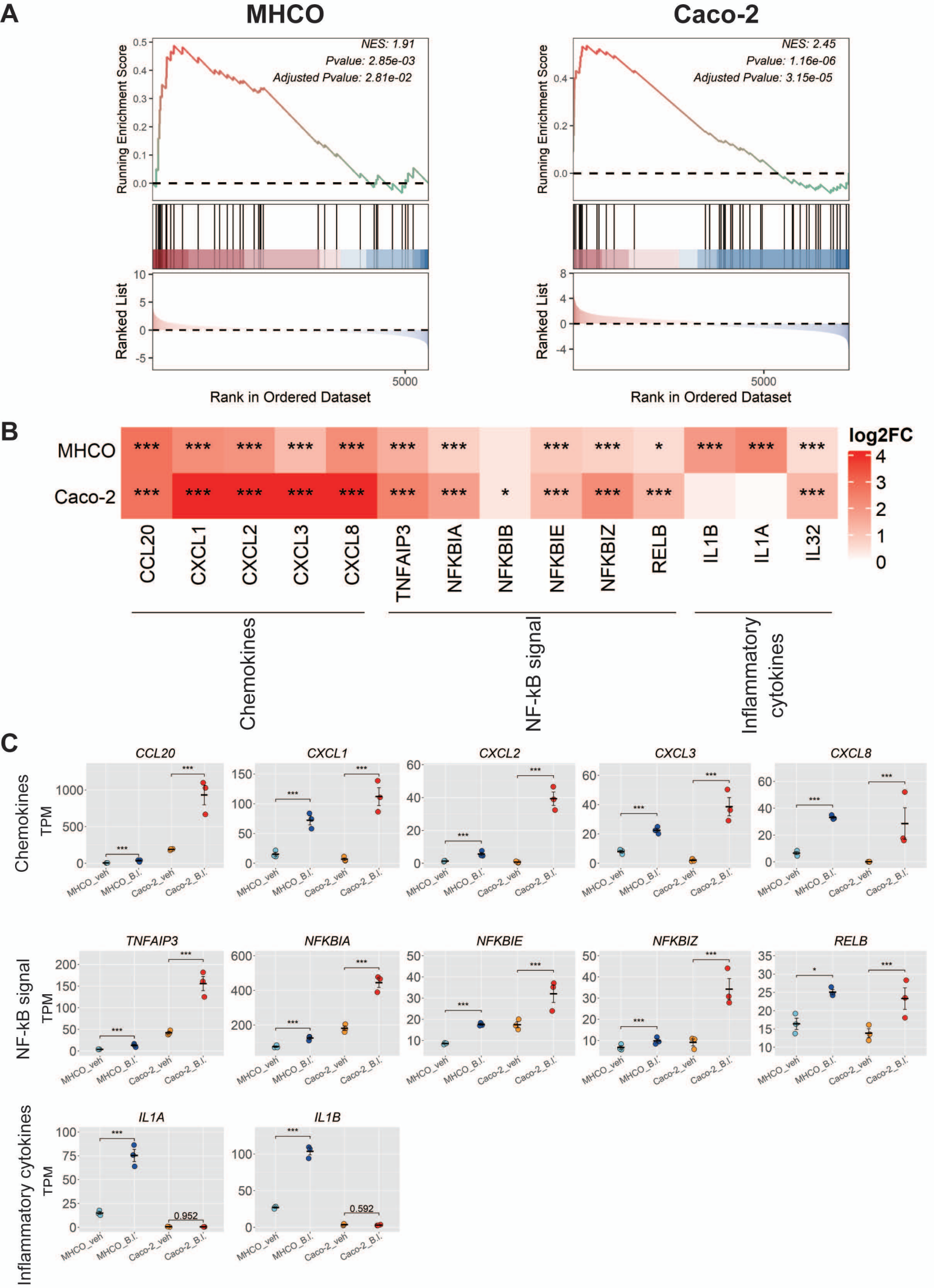

Figure 6. Sen et al.

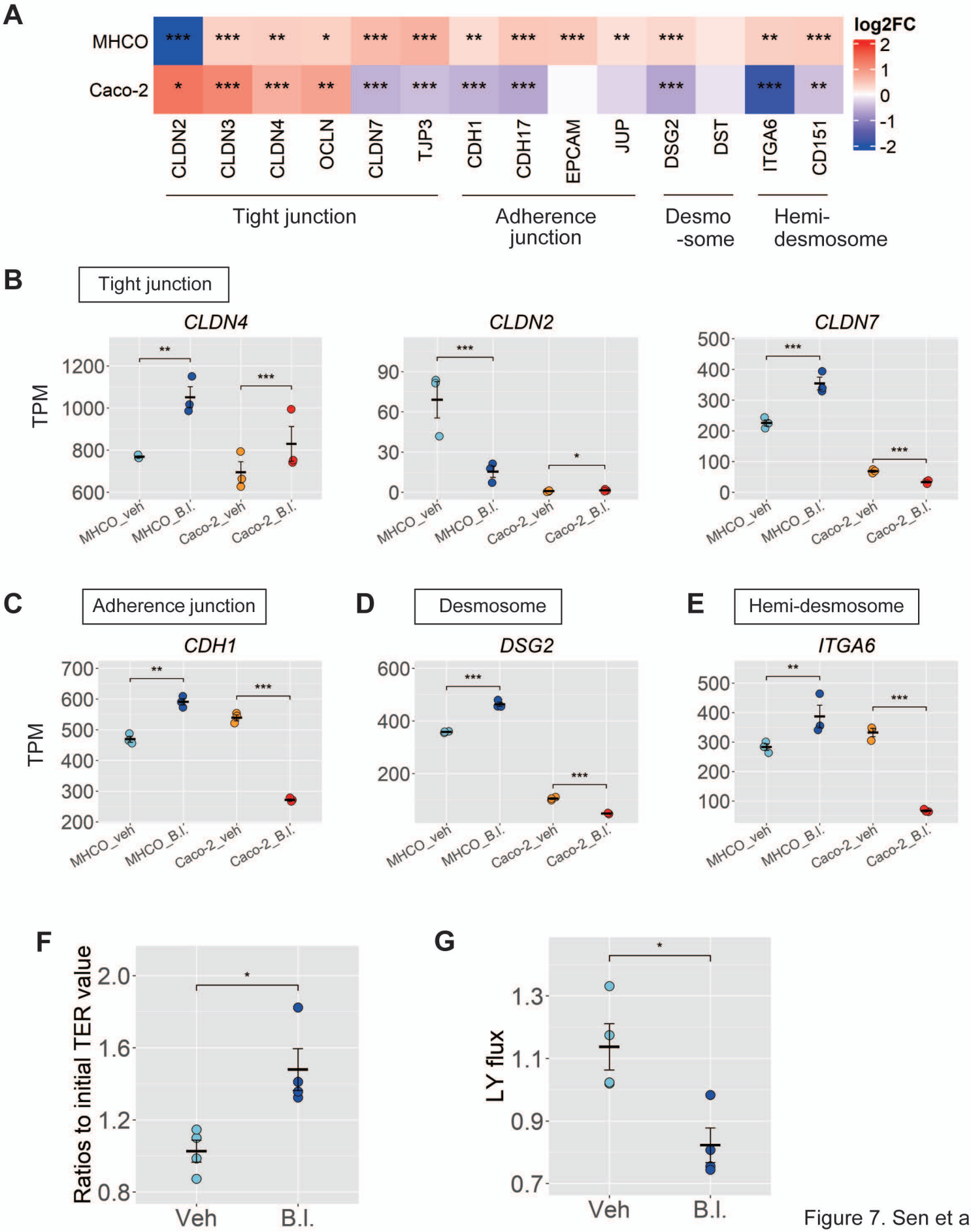

Figure 7. Sen et al.